PHYSICAL REVIEW D **93,** 075008 (2016)

Bulk Randall-Sundrum models, electroweak precision tests, and the 125 GeV Higgs

Abhishek M Iyer,[1,*] K. Sridhar,[1,†] and Sudhir K. Vempati[2,‡]

[1]*Department of Theoretical Physics, Tata Institute of Fundamental Research, Homi Bhabha Road, Colaba, Mumbai 400 005, India*

[2]*Centre for High Energy Physics, Indian Institute of Science, Bangalore 560012, India*

(Received 29 January 2016; published 4 April 2016)

We present up-to-date electroweak fits of various Randall-Sundrum (RS) models. We consider the bulk RS, deformed RS, and the custodial RS models. For the bulk RS case we find the lightest Kaluza-Klein (KK) mode of the gauge boson to be ∼8 TeV, while for the custodial case it is ∼3 TeV. The deformed model is the least fine-tuned of all which can give a good fit for KK masses < 2 TeV depending on the choice of the model parameters. We also comment on the fine-tuning in each case.

DOI: 10.1103/PhysRevD.93.075008

I. INTRODUCTION

The discovery of the Higgs boson at ∼125 GeV has firmly established the status of the Higgs mechanism as the theory of electroweak symmetry breaking physics. In addition, it also fixes one of the main unknown inputs of electroweak precision fits. Electroweak precision measurements put very important and sometimes very strong constraints on new physics models. In the present work we focus on the Randall-Sundrum (RS) model [1] and its variations. We update the constraints on the lightest Kaluza-Klein (KK) modes of RS scenarios in light of the discovery of the Higgs mass and improved measurements of the W-boson mass (m_w) and top mass (m_t). Electroweak precision constraints played an important role in the evolution of RS models and their phenomenology.[1] In the original standard proposal all the Standard Model (SM) fields are localized on the IR brane.

Later motivated by gauge coupling unification, gauge fields were moved to the bulk while keeping the Higgs and the fermion fields on the brane [4]. In both cases large contributions to the oblique S and T parameters were noted [5], resulting in bounds on the first KK mass in excess of 30 TeV [6–11]. Moving the fermions into the bulk served the following two purposes.

(1) It offered an elegant solution to the Yukawa hierarchy puzzle achieved by localizing the fermions at different points in the bulk, resulting in interesting flavor phenomenology in the hadronic sector [12–16] and the leptonic sector [13,17–29]. For a detailed description of RS phenomenology with bulk fields, see Refs. [2,30].

(2) The constraints on the gauge KK states from the S parameter are significantly weakened as all the light fermions except the top are localized away from the IR brane and Higgs.

The constraints from the T parameter, however, remain strong as the Higgs doublet is localized near the IR brane which is necessary for the solution to the hierarchy problem. In view of this, the following extensions were proposed. a) Models with bulk custodial symmetry [31]: The bulk gauge group in question is $\mathrm{SU}(2)_L \times \mathrm{SU}(2)_R \times \mathrm{U}(1)_X$. In this case the additional corrections to the T parameter due to new KK gauge bosons cancel the volume-enhanced contributions due to the KK states of the SM gauge bosons. The T parameter vanishes at tree level and the limits on the KK mass of the first gauge boson are mainly due to the S parameter. A straightforward estimation of the S parameter results in a lower bound on the first KK mass of ∼4 TeV for the point to lie inside the 3σ region in Fig. 1. Taking into account the loop corrections to the T parameter (in scenarios with Zbb protection), it was found that one can lower the mass of the first KK gauge boson to around 3 TeV at 3σ. An additional alternative is to consider custodial models with gauge-Higgs unification which can address the little hierarchy problem. [32]. A global fit to the precision observables in such models was performed in Ref. [33]. Scenarios with bulk Higgs were considered in Ref. [34]. b) Models with a deformed metric [35–37]: In this setup the bulk geometry is RS-like [anti–de Sitter (AdS)] near the UV brane, while there is a deviation from AdS geometry near the IR brane. Depending on the model parameters this often results in a smaller volume factor as compared to the original RS setup. In Ref. [38] the authors performed a fit to the data for different values of the Higgs mass and evaluated the fine-tuning required to fit that particular Higgs mass. In Ref. [39] the authors studied the implications of the one-loop corrections to the T parameter on the fits. c) Models with brane-localized kinetic terms for the gauge bosons [40]. There were several previous analyses where the impact of bulk fields on

*abhishek@theory.tifr.res.in
†sridhar@theory.tifr.res.in
‡vempati@cts.iisc.ernet.in

[1]For a recent review see Refs. [2,3].

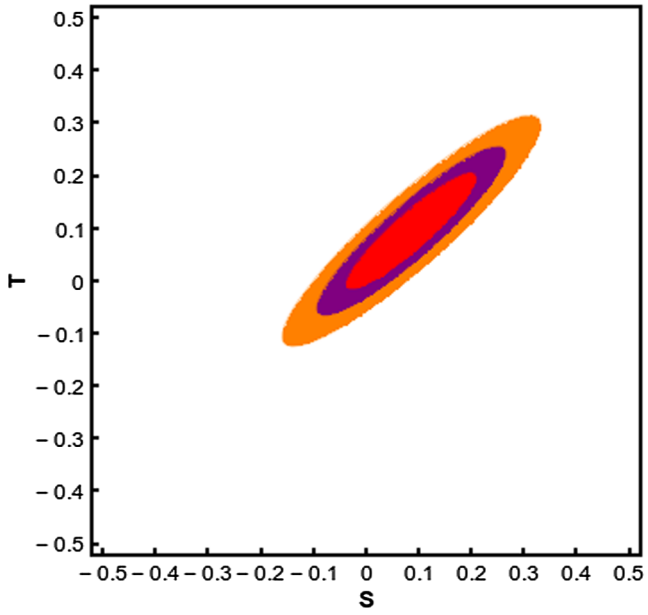

FIG. 1. The red, blue, and orange regions denote the 68%, 95%, and 99% confidence level allowed regions in the S-T parameter space.

oblique observables was studied. With bulk fermions, the dominant constraint on the KK mass is due to the T parameter which is enhanced due to the mixing of the zero-mode gauge bosons with the KK modes. This mixing is governed by the Higgs vacuum expectation value (VEV). As noted in Ref. [26], these constraints can be ameliorated with a Higgs VEV that is not strongly localized near the IR brane, which in turn reduces the zero-KK mode mixing. This setup is particularly useful in a model with a deformed-RS metric, where the KK constraints on the lowest KK masses can be reduced to ∼2.5 TeV. In Ref. [41] the authors, while updating the bounds on the KK masses from precision electroweak data, also discussed the impact of the future measurements of rare K and B decays on the parameter space of the model. They also discussed the correlation between the these flavor measurements and the limits from direct searches for current and future runs of the LHC. General composite Higgs models were discussed in Ref. [42], of which RS was considered as an example. While discussing the trilinear and quartic anomalous gauge couplings in these scenarios, they quoted limits on the mass of the KK gauge resonance due to precise values of the S and T parameters. In the absence of brane kinetic terms, the constraint on custodial models with a brane Higgs was about 7 TeV, while this could be lowered to 6.6 TeV for a pseudo-Nambu-Goldstone Higgs at the 95% C.L. Models with bulk Higgs were also considered in Ref. [34], where a detailed analysis correlating signal strengths for different production mechanisms and decay channels was performed as a function of the anarchic bulk Yukawa parameter, KK masses, and the extent of the compositeness of the Higgs operator. In Ref. [43] the authors showed that the inclusion of higher-dimensional operators in the bulk and on the branes can significantly reduce the constraints on the T parameter. These operators only require $\mathcal{O}(1)$ coefficients, and do not contribute much to the other electroweak parameters. We focus our attention on scenarios a) and b) of the extensions to the RS model. In both the scenarios the brane mass parameter of the Higgs doublet plays an important role in determining the constraint on the first KK mass of the gauge boson. Additionally, with the precise measurement of the Higgs mass, the extent of fine-tuning is related to the brane mass parameter b [36–38]. We make explicit the interplay between the fine-tuning required to fit the Higgs boson mass and the b parameter which gives the best fit to the electroweak observables. Using the expansion formalism of Ref. [44] we determine the best-fit points for the model parameters by using the standard χ^2 analysis. We find that the KK mass of the first gauge boson is lower than what was obtained in earlier analyses when naive bounds from the evaluation of S and T parameters were taken into account.

The paper is organized as follows. In Secs. II and III we outline the formalism of Ref. [44], thus providing the necessary background for the analysis. In Sec. IV we briefly review the bulk RS model and study the bulk RS model with no additional gauge symmetries. In Secs. V and VI we analyze the RS model with a deformed metric and custodial symmetry, respectively. We conclude in Sec. VII.

II. EXPANSION FORMALISM AND THE SM

In this section we briefly review the expansion formalism of Ref. [44] which we use for our analysis. There are numerous observables in the Standard Model whose values have been very well measured. These observables are in general a function of the following Lagrangian parameters:

$$p_{k'} \equiv \{g_i, y_t, v, \lambda\}, \tag{1}$$

where g_i are the gauge couplings, y_t is the top quark Yukawa coupling, v is the VEV, and λ is the quartic coupling. These parameters are referred to as the "input parameters." The ith observable $\hat{O}_i^{\rm SM}$ in the SM can be expressed as a function of these parameters as

$$\hat{O}_i^{\rm SM}(\{p_{k'}\}) = \hat{O}_i^{\rm ref} + \sum_{k'} \frac{\partial \hat{O}_i^{\rm SM}}{\partial p_{k'}} (p_{k'} - p_{k'}^{\rm ref}) + \cdots, \tag{2}$$

where the $\cdots$ denote higher orders. $\{p_{k'}^{\rm ref}\}$ is the set of Lagrangian parameters chosen at a reference value $p_{k'}^{\rm ref}$ at which the evaluated expressions for the SM observables match closely with experiment, and $\hat{O}_i^{\rm ref} = \hat{O}_i^{\rm SM}(\{p_{k'}^{\rm ref}\})$. Thus the expansion in Eq. (2) is about the reference values $p_{k'}^{\rm ref}$ and $p_{k'}$ is the allowed deviation about the reference values.

TABLE I. Experimentally measured central values for the input and output observables along with the standard deviation.

Input observables	m_Z	91.1876(21)	[47]	G_F	$1.1663787(6) \times 10^{-5}$	[48]
	$\alpha(m_Z)$	$7.81592(86) \times 10^{-3}$	[48]	$m_t(m_t)$	173.34(75)	[49]
	$\alpha_s(m_Z)$	0.1185(6)	[48]	m_H	125.9(4)	[48]
Output observables	m_W	80.385(15)	[50]	Γ_Z	2.4952(23)	[47]
	$\sigma_{\rm had}$	41.541(37)	[47]	R_e	20.804(50)	[47]
	R_μ	20.785(33)	[47]	$R_{\rm tau}$	20.764(45)	[47]
	R_b	0.21629(66)	[47]	R_c	0.1721(30)	[47]
	$\sin^2\theta_e$	0.23153(16)	[47]	$\sin^2\theta_b$	0.281(16)	[47]
	$\sin^2\theta_c$	0.2355(59)	[47]	A^e_{FB}	0.0145(25)	[47]
	A^b_{FB}	0.0992(16)	[47]	A^c_{FB}	0.0707(35)	[47]
	A_b	0.923(20)	[47]	A_c	0.670(27)	[47]

TABLE II. Best-fit values for the input and output observables for the SM fit with $\chi^2_{\rm min} = 24.54$.

Input observables	m_Z	91.188	G_F	1.16638×10^{-5}
	$\alpha(m_Z)$	7.81589×10^{-3}	$m_t(m_t)$	173.59
	$\alpha_s(m_Z)$	0.118567	m_H	125.89
	m_W	80.366 ± 0.005	Γ_Z	2.4957 ± 0.0006
Output observables	$\sigma_{\rm had}$	41.472 ± 0.04	R_e	20.7427 ± 0.03
	R_μ	20.7428 ± 0.03	$R_{\rm tau}$	20.7897 ± 0.03
	R_b	0.215822 ± 0.00005	R_c	0.17209 ± 0.000007
	$\sin^2\theta_e$	0.23161 ± 0.000002	$\sin^2\theta_b$	0.2329 ± 0.00001
	$\sin^2\theta_c$	0.2315 ± 0.000002	A^e_{FB}	0.0160 ± 0.000004
	A^b_{FB}	0.1025 ± 0.00002	A^c_{FB}	0.0732 ± 0.00001
	A_b	0.9346 ± 0.00005	A_c	0.6675 ± 0.000008

The Lagrangian parameters, however, are not measured directly, but rather are extracted from the measurements of certain observables. As a result it seems logical to reexpress the SM observables in terms of a few accurately measured observables which will now serve as the input. One such list of input observables is[2]

$$\hat{O}_{k'} \equiv \{m_Z, m_H, G_F, \alpha(m_Z), \alpha_s(m_Z), m_t(m_t)\}. \tag{3}$$

In terms of the input observables, Eq. (2) can be reexpressed as follows:

$$\hat{O}_i^{\rm SM}(\{\hat{O}_{k'}\}) = \hat{O}_i^{\rm ref} + \sum_{k'} \frac{\partial \hat{O}_i^{\rm SM}}{\partial \hat{O}_{k'}} (\hat{O}_{k'} - \hat{O}_{k'}^{\rm ref}) + \cdots, \tag{4}$$

where $\hat{O}_{k'}^{\rm ref}$ is the experimentally measured central value of the input observable and $\hat{O}_{k'}$ quantifies the deviation from the central value. Thus the deviation in $\hat{O}_i^{\rm SM}$ can be expressed in terms of the experimental deviation of the input observables from their central values. The relative deviation can be defined as

$$\bar{\delta}^{\rm SM}\hat{O}_i(\{\hat{O}_{k'}\}) = \frac{\hat{O}_i^{\rm SM}(\{\hat{O}_{k'}\}) - \hat{O}_i^{\rm ref}(\{\hat{O}_{k'}^{\rm ref}\})}{\hat{O}_i^{\rm ref}}. \tag{5}$$

Defining

$$c_{ik'} = \frac{\hat{O}_{k'}^{\rm ref}}{\hat{O}_i^{\rm ref}} \frac{\partial \hat{O}_i^{\rm SM}}{\partial \hat{O}_{k'}}, \tag{6}$$

we can express the relative deviation in Eq. (5) in the ith observable, due to the deviation from the central value of the input observables as

$$\bar{\delta}O_i^{\rm SM} = \sum_{i'} c_{ii'} \delta \hat{O}_{i'}^{\rm SM}. \tag{7}$$

Using this, Eq. (4) can be rewritten as

$$\hat{O}_i^{\rm SM}(\{\hat{O}_{k'}\}) = \hat{O}_i^{\rm ref}(1 + \hat{\delta}^{\rm SM}\hat{O}_i). \tag{8}$$

The deviation of all the SM observables can be quantified by constructing a χ^2 statistic defined as

$$\chi^2(\hat{O}_{k'}) = \sum_i \left[\frac{\hat{O}_i^{\rm SM}(\hat{O}_{k'}) - \hat{O}_i^{\rm expt}}{\delta \hat{O}_i^{\rm expt}} \right]^2. \tag{9}$$

[2]A subset of these observables can be used to "determine" the input parameters.

It should be noted that while constructing the χ^2 we assume that there is no correlation [45] between the output observables. However, we note that taking into account the correlation matrix for the output observables will not significantly change the results of our analysis. The central values and the allowed deviation for the input and output observables are given in Table I. Using the Z pole observables and the W mass as the output observables, we minimize the χ^2 function in Eq. (9) by varying the input observables within the experimentally allowed deviation given in Table I. The minimization is performed using the method from Ref. [46]. We obtain $\chi^2_{\rm min} = 24.54$ with the corresponding best-fit values for the input observables given in Table II.

III. NEW PHYSICS

The expansion formalism presented in Sec. II can be extended to include new physics effects. Assuming the nature of new physics is such that it mostly modifies the oblique parameters, the new physics effects can be parametrized by the introduction of higher-dimension operators in the Lagrangian. These operators can give corrections to any of the input and the output observables.[3] In the presence of new physics, Eq. (7) becomes

$$\delta^{NP}\hat{O}_i^{th}(\{\hat{O}_{k'}\}, NP) = \bar{\delta}\hat{O}_i^{\rm SM} + \zeta_i, \tag{10}$$

where $\zeta_i(\{\hat{O}_{k'}\}, NP) \equiv \frac{\delta^{NP}\hat{O}_i^{th}(\{\hat{O}_{k'}\}, NP)}{\hat{O}_i^{\rm ref}}$ parametrizes the relative contribution to the ith observable due to higher-dimension operators. Using Eq. (7), Eq. (10) can be written as

$$\begin{aligned}\delta^{NP}\hat{O}_i^{th}(\{\hat{O}_{k'}\}, NP) &= \sum_{i'} c_{ii'}\delta\hat{O}_{i'}^{\rm SM} + \zeta_i \\ &= \sum_{i'} c_{ii'}\delta\hat{O}_{i'}^{th} + \bar{\delta}^{NP}\hat{O}_i,\end{aligned} \tag{11}$$

where $\bar{\delta}^{NP}\hat{O}_i = \zeta_i - \sum_{i'} c_{ii'}\zeta_{i'}$. Here the superscript "$th$" denotes the SM in addition to new physics. Note that from Eq. (6), the matrix of coefficients $c_{ik'}$ is a unit matrix for the input observables, i.e., $c_{i'k'} = \delta_{i'k'}$. Thus any new physics effects on the input observables are adjusted such that the net shift is zero, which is apparent in Eq. (11). This adjustment is however propagated in the evaluation of the output observables through Eq. (11).

In many scenarios, new physics is such that the dominant contribution to the various SM observables is only through the self-energy corrections to the various gauge boson propagators given below:

$$\pi_{\alpha\beta} \equiv \{\pi_{ZZ}, \pi'_{ZZ}, \pi_{\gamma Z}, \pi'_{\gamma\gamma}, \pi_{WW}, \pi^0_{WW}\}. \tag{12}$$

The primed quantities denote differentiation with respect to q^2, where q is the four-momentum. Note that the corrections to the fermion coupling to the gauge bosons are universal. In this case the new physics contribution to the input observables in Eq. (11) can be reexpressed as

$$\delta^{NP}\hat{O}_i^{th} = \sum b_{i,\alpha\beta}\delta^{NP}\pi_{\alpha\beta}, \tag{13}$$

where it is understood that the sum extends over the list in Eq. (12) while the coefficients $b_{\alpha\beta}$ were evaluated in Ref. [44].

In such models the corrections to the gauge boson propagators can be encoded in the oblique parameters S and T [5,55].[4] These oblique parameters are related to the new physics effects to the self-energy correction as follows [56];

$$\begin{aligned}\delta^{NP}\pi_{ZZ} &= -\alpha(m_Z)T + \frac{\alpha(m_Z)}{2}S, \\ \delta^{NP}\pi'_{ZZ} &= \frac{\alpha(m_Z)}{2}S, \\ \delta^{NP}\pi_{\gamma Z} &= -\frac{\alpha(m_Z)}{4\sin^2\theta_W}\cos 2\theta_W \tan\theta_W S, \\ \delta^{NP}\pi'_{\gamma\gamma} &= -\frac{\alpha(m_Z)}{2}S.\end{aligned}$$

We use Eq. (13) in Eq. (11) to construct the χ^2 for the output observables at the Z peak along with the W mass. Using the results of the analysis in Ref. [44], the expression for the χ^2 statistic defined in Eq. (9) is given as

$$\begin{aligned}\chi^2 = {} & 25.0898 + 1102.39S^2 + 28.746S - 72.0085T \\ & - 2256.69ST + 1377.07T^2.\end{aligned} \tag{14}$$

The input observables were fixed to their experimentally measured central values while obtaining the above expression. Using this we obtain the S-T plot in Fig. 1 in which the 68%, 95%, and 99% confidence level allowed regions are depicted by the red, blue, and orange regions, respectively. Our analysis is performed by fixing $U = 0$. Additionally the best-fit point for $m_h^{\rm ref} = 125$ GeV and $m_t^{\rm ref} = 173$ GeV was obtained to be $S = 0.08 \pm 0.1$ and $T = 0.09 \pm 0.1$, and the correlation coefficient between the S and the T parameter is $+0.89$. In addition to S and T, the other floating-point parameters were $m_Z = 91.1876 \pm 0.0021$, $\alpha_s(M_Z) = 0.1185 \pm 0.0006$, and $\alpha(M_Z^2) = 7.81596(86) \times 10^{-3}$. These results are to be compared with the GFITTER analysis [57] where the $\{m_Z, \alpha, \Delta\alpha\}$ were considered as the floating-point parameters with $\Delta\alpha(M_Z^2) = 0.02757 \pm 0.0001$. They

[3] In the calculations used for our analysis only tree-level effective theory operators are considered. Things could get more stringent if one-loop effective theory operators are considered [51–53]. For a detailed analysis of precision observables using the Standard Model effective field theory, see Ref. [54].

[4] The contribution to U is suppressed as only dimension-eight operators contribute to it.

obtained $S = 0.06 \pm 0.09$ and $T = 0.1 \pm 0.07$ with a correlation coefficient $+0.91$.

For a particular model of new physics, the oblique parameters S and T depend on the model parameters. A given set of model parameters is valid only if the corresponding S, T observables computed for that set lie at least within the orange ellipse in Fig. 1. Thus a very small contribution (for example, to the S parameter) would require T to also be very small so as to lie within the bottom left portion of the ellipse. However an increasing S can admit larger values of the T parameter, corresponding to moving towards the top right portion of the ellipse. Thus we can use Fig. 1 to constrain the model parameters. We now use this analysis to obtain constraints on various Randall-Sundrum models.

IV. RANDALL-SUNDRUM MODELS

The Randall-Sundrum model is a model of a single extra dimension compactified on an S_1/Z_2 orbifold [1]. The five-dimensional gravity theory is defined by the following line element:

$$ds^2 = e^{-2A(y)}\eta_{\mu\nu}dx^\mu dx^\nu - dy^2. \tag{15}$$

Two opposite-tension branes are located at the two fixed points of the orbifold. The space between the branes is endowed with a large negative bulk cosmological constant making it a slice of AdS. The presence of brane-localized sources of energy results in zero cosmological constant being induced on the branes. In the original setup $A(y) = ky$, where k is the reduced Planck scale. Identifying the scale of physics on the $y = 0$ brane as $M_{\rm IR}$, the effective UV scale induced at the $y = \pi R$ brane owing to geometry is given as

$$M_{\rm IR} = e^{-kR\pi}k, \tag{16}$$

where R is the compactification radius. Choosing $kR \sim 12$ will result in $M_{\rm IR} \sim 200$ GeV owing to large exponential warping. Any radiative instability to the masses of fundamental scalars in the theory can be warped down to the electroweak scale, thus solving the gauge hierarchy problem. In the original setup, with the exception of gravity all the SM fields were localized on the brane at $y = y_1 = \pi R$, also referred to as the IR brane. Here we consider a generalization of the original setup where particles of all types of spin are allowed to propagate in the bulk.

A bulk field $\Psi^s(x^\mu, y)$ with spin s can be expanded in the KK basis as follows:

$$\Psi^s(x^\mu, y) = \frac{1}{\sqrt{\pi R}}\sum_{n=0}^{\infty}\psi_s^{(n)}(x^\mu)f_s^{(n)}(y). \tag{17}$$

The zero modes for the fields are identified as the SM fields. While the zero modes for the gauge bosons are flat at leading order, the ones for the scalars and the fermions are controlled by the brane and bulk mass terms, respectively. They are parametrized as $m^s_{\rm brane} = bk$ and $m^f_{\rm bulk} = ck$, where b, c are dimensionless $\mathcal{O}(1)$ quantities. The normalized profiles for the fields are given as

$$\begin{aligned} f_0^{(0)}(b, y) &= \sqrt{\frac{2(b-1)kR\pi}{e^{2(b-1)kR\pi} - 1}}e^{(b-1)ky}, \\ f_{1/2}^{(0)}(c, y) &= \sqrt{\frac{(1-2c)kR\pi}{e^{(1-2c)kR\pi} - 1}}e^{(0.5-c)ky}, \\ f_1^{(0)}(y) &= 1, \end{aligned} \tag{18}$$

where the normalization conditions are given as

$$\frac{1}{\pi R}\int_0^{\pi R}(f_s^{(0)}(y))^2 dy = 1. \tag{19}$$

$c < 0.5$ and $b > 1$ ($c > 0.5$ and $b < 1$) correspond to the fields being localized towards the IR (UV) brane, respectively. The KK modes of all fields are however localized near the IR brane. We note here that while the profiles of the gauge boson fields are flat at leading order, they receives corrections due to the mixing of the KK mode with the zero mode. The mixing is proportional to the VEV and is given as

$$a_{01} = \frac{v^2}{(kR\pi)M_{KK}^2}\int_1^{z_{\rm IR}} z^2 f_0^{(0)}(z)^2 f_1(z)^{(0)} f_1(z)^{(1)}, \tag{20}$$

where $z = e^{kRy}$ is the conformal coordinate. $f_{0,1}^{(0)}$ are given in Eq. (18), while $f_1^{(1)}$ is the profile of the first KK mode of the gauge boson. A detailed review about bulk RS models can be found in Refs. [2,3]. Thus diagonalizing the mass matrix of KK modes and the zero mode will result in the lightest state (identified as the SM boson) having a small KK component proportional to Eq. (20). As a result the coupling of the fermions to the SM boson will have a nonuniversal component which is a function of its localization parameter c. The c parameters will be in general different for different fermionic generations to generate the required hierarchy in the Yukawa parameters. For the light fields with the exception of the top it is fair to assume $c > 0.5$ to reduce the overlap with the Higgs. For $c > 0.5$, the nonuniversal component of the coupling is very small and can be neglected [2,58]. This is enough to evade bounds from flavor-changing neutral current (FCNC) processes which can occur at tree level.

The solution of the hierarchy problem requires the Higgs zero mode to be localized very close to the IR brane. It corresponds to a choice $b \geq 2$ for the brane

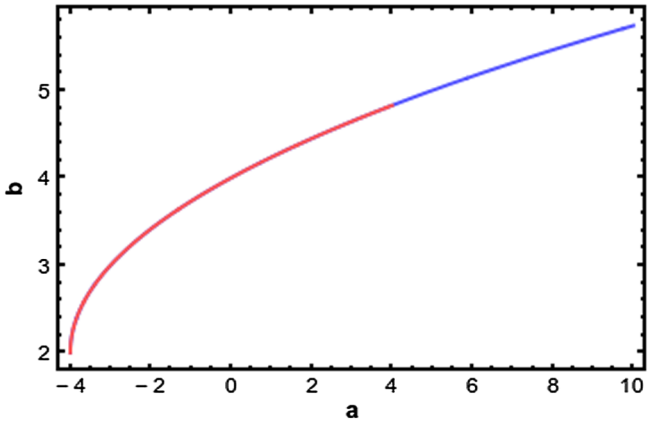

FIG. 2. Maximum allowed value of b for $\frac{k}{M_{pl}} = 0.25$ (red) and $\frac{k}{M_{pl}} = 0.1$ (blue).

mass parameter [37,59].[5] For a bulk scalar field with a massless zero mode the brane mass parameter b is related to the bulk mass parameter a as[6]

$$b = 2 \pm \sqrt{4 + a}. \tag{21}$$

Henceforth, we will drop the $b = 2 - \sqrt{4+a}$ solution as it will never lead to a $b \geq 2$ necessary for the solution to the hierarchy problem. The zero mode increasingly becomes sharply localized near the IR brane as b increases. However, an increase in b is only facilitated by the corresponding increase in $|a|$. Depending on the value of $\frac{k}{M_{pl}}$, the bulk mass parameter cannot be increased indefinitely as the product ak will become greater than the five-dimensional Planck scale. Figure 2 shows a plot of b as a function of a. Depending on the value of $\frac{k}{M_{pl}}$, the plot is terminated on the right at which $ak = M_{\rm Pl}$. For instance, for $\frac{k}{M_{pl}} = 0.1$, the plot (blue curve) is terminated at $b = 5.74$, while for $\frac{k}{M_{pl}} = 0.25$ the plot (red curve) is terminated $b = 4.82$.

Thus the case with a brane-localized Higgs will be treated separately and not as a limiting case where the bulk Higgs field tends to a brane-localized one.

We now proceed to study the impact of electroweak precision tests in various RS models.

A. Bulk Higgs with no additional symmetries

This model is the same setup as that discussed above. All the fermionic fields except the top are localized near the UV brane. This is sufficient to fit the masses of all fermions except the top. Due to the localization of all the fermions near the UV brane, the vertex corrections are very small and universal, and thus the new physics effects can be parametrized in terms of the oblique operators S and T which are given as [36–38]

$$\alpha T = \frac{\sin^2\theta_W m_Z^2 y_1 k^2 e^{-2kR\pi}}{\Lambda_{\rm IR}^2}(\alpha_{hh} - 2\alpha_{hf} + \alpha_{ff}),$$
$$\alpha S = \frac{8\sin^2\theta_W \cos^2\theta_W m_Z^2 y_1 k^2 e^{-2kR\pi}}{\Lambda_{\rm IR}^2}(\alpha_{ff} - \alpha_{hf}), \tag{22}$$

where y_1 denotes the position of the IR brane and α_{ij} are parameters involving the bulk propagators of the bulk gauge fields with $(++)$ boundary conditions, where $+$ denotes the Neumann boundary condition. They are given as [37,61]

$$\alpha_{hh} = \int e^{2A(y)}\left(\Omega_h - \frac{y}{y_1}\right)^2,$$
$$\alpha_{hf} = \int e^{2A(y)}\left(\Omega_h - \frac{y}{y_1}\right)\left(\Omega_f - \frac{y}{y_1}\right),$$
$$\alpha_{ff} = \int e^{2A(y)}\left(\Omega_f - \frac{y}{y_1}\right)^2, \tag{23}$$

where $\Omega_{f,h}(y) = \frac{1}{y_1}\int_0^y dy f_{f,h}^2(y)$ and the profiles $f's$ are given by Eq. (18). For the case where the fermions are localized on the UV brane, $\Omega_f = 1$. These coefficients are a function of the localization of the zero mode of the fermionic and Higgs fields. For a fixed KK scale, the coefficients increase as the fields move closer to the IR brane due to a larger overlap of the zero mode with the KK modes.

For the oblique T parameters, the coefficient α_{hh} also contributes in addition to $\alpha_{hf,ff}$. Owing to the localization of the Higgs very close to the IR brane, α_{hh} will be enhanced as compared to $\alpha_{hf,ff}$, which is smaller as the fermions are closer to the UV brane. As a result in this scenario the contributions to the T parameter are large. In

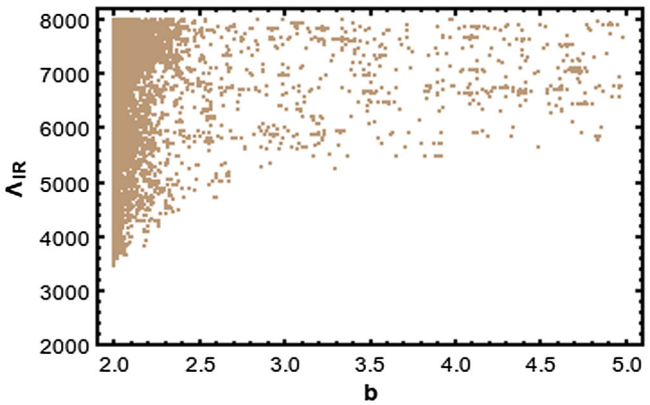

FIG. 3. 3σ allowed parameter space in the $b - \Lambda_{\rm IR}$ plane for regular bulk RS. $\Lambda_{\rm IR}$ is in GeV.

[5]The realization of electroweak symmetry breaking also requires $b > 2$ [60].

[6]The bulk scalar mass is parametrized as $m^s_{\rm bulk} = ak$.

TABLE III. Fit values for the input and output observables with a bulk Higgs. Input observables are free in the fit and are varied within their 1σ allowed experimental deviation. $b = 2.00$ and $m^1_{kk} = 8.3$ TeV are obtained for the fit.

Input observables	m_Z	91.1813	G_F	1.1663784×10^{-5}
	$\alpha(m_Z)$	7.81611×10^{-3}	$m_t(m_t)$	173.05
	$\alpha_s(m_Z)$	0.119101	m_H	126.3
Output observables	m_W	80.411	Γ_Z	2.4983
	$\sigma_{\rm had}$	41.479	R_e	20.7472
	R_μ	20.7473	$R_{\rm tau}$	20.7941
	R_b	0.2158	R_c	0.1712
	$\sin^2\theta_e$	0.2313	$\sin^2\theta_b$	0.2327
	$\sin^2\theta_c$	0.2312	A^e_{FB}	0.0164
	A^b_{FB}	0.1038	A^c_{FB}	0.0742
	A_b	0.9347	A_c	0.6683
Model Parameters	b	2.00	m^1_{kk}	8.3 TeV

TABLE IV. Fit values for the input and output observables. Input observables are free in the fit and are varied within their 1σ allowed experimental deviation. $m^1_{kk} = 13.6$ TeV is obtained for the fit.

Input observables	m_Z	91.1856	G_F	$1.16637854 \times 10^{-5}$
	$\alpha(m_Z)$	7.816649×10^{-3}	$m_t(m_t)$	172.33
	$\alpha_s(m_Z)$	0.118657	m_H	126.295
	m_W	80.402	Γ_Z	2.4976
Output observables	$\sigma_{\rm had}$	41.477	R_e	20.744
	R_μ	20.744	$R_{\rm tau}$	20.7916
	R_b	0.2158	R_c	0.17229
	$\sin^2\theta_e$	0.2314	$\sin^2\theta_b$	0.2327
	$\sin^2\theta_c$	0.2313	A^e_{FB}	0.0164
	A^b_{FB}	0.1036	A^c_{FB}	0.07412
	A_b	0.9347	A_c	0.6682

this case the oblique observables primarily depend on two parameters:

(a) The localization parameter b for the bulk Higgs field.
(b) The first KK scale of the gauge boson.

To extract the parameter space of these two parameters (which are consistent with the constraints on the S and T parameters) a scan is performed over the following ranges:

$$b \equiv [2, 5], \qquad \Lambda_{\rm IR} \equiv [1250, 10000]. \tag{24}$$

Figure 3 shows the 3σ region in the $b - \Lambda_{\rm IR}$ plane. The first KK mass of the gauge boson is related to the IR scale as $m^{(1)}_{KK} \sim 2.44\Lambda_{\rm IR}$. We see $\Lambda_{\rm IR}$ is lowered as b approaches 2, corresponding to a shifting of the Higgs away from the IR brane. However, $b \geq 2$ must be maintained for the model to serve as a solution to the hierarchy problem [37,59]. Table III gives the fit values when all input observables along with b and $\Lambda_{\rm IR}$ are varied simultaneously to minimize the χ^2 in Eq. (9). From the plot in Fig. 3 we find that the lowest value of $\Lambda_{\rm IR}$ possible is around 3.4 TeV, corresponding to a first KK mass for the gauge boson of around 8 TeV. The plot is highly concentrated around $b = 2$ since the coupling of the SM fields to the KK states is small as compared to higher values of b. This point corresponds to the case where the mass of the first KK gauge boson is minimum.

We finally note that for the brane-localized case, a minimum KK mass of 13.6 TeV is required for the model to be consistent with the data. The fit values for the input and the output observables are given in Table IV.

It is to be noted that KK scales in excess of 20 TeV are required when constraints from FCNCs like $\mu \to e\gamma$ are taken into account [27]. The implementation of bulk flavor symmetries with the imposition of the minimal flavor violation ansatz helps to substantially reduce the KK mass to around ~3 TeV [12,23,62,63].

Fine-tuning: It is well known that the requirement of a massless zero mode for the bulk scalar field requires the bulk mass $m_{\rm bulk} = ak$ and the brane mass $m_{\rm brane} = bk$ to be related by the following relation[7]:

$$m_{\rm brane} = 2k + \sqrt{4k^2 + m^2_{\rm bulk}}. \tag{25}$$

Any misalignment between the brane and the bulk masses will result in a nonzero mass for the zero mode. In a realistic model with electroweak symmetry breaking, the

[7]The relation $m_{\rm brane} = 2k - \sqrt{4k^2 + m^2_{\rm bulk}}$ is relevant for a Higgs field localized away from the IR brane and is not relevant to the discussion here.

Higgs boson is massive and is related to the misalignment as [36,37,64]

$$m_H^2 = 4(b-1)(m_{\text{brane}} - m'_{\text{brane}})\frac{\Lambda_{\text{IR}}^2}{k}, \tag{26}$$

where $m'_{\text{brane}} = bk$ is the value of the brane mass when the zero mode is massless. As given in Table III, $\Lambda_{\text{IR}} = 2.41$ TeV in order for the model to be consistent with the electroweak precision data. As a result, for $b = 2$ a cancellation up to the fourth decimal between m'_{brane} and m_{brane} is required to fit a Higgs mass of 126 GeV. The level of tuning increases as the Higgs field is pushed closer to the IR brane, corresponding to an increase in b. Due to a direct dependence on the brane mass parameter b [36,37,65], it is fair to expect that the Higgs boson mass is best fit by $b \sim 2$. In the dual theory this corresponds to the Higgs field being a partial composite state with a relevant coupling between the source and the conformal field theory (CFT) sectors. As b increases, this coupling increases and the state is fully composite of the CFT, thus recovering the original RS setup.

V. DEFORMED RS MODEL

The expression for the S and T parameters in Eq. (22) can be reexpressed as [36,37]

$$\alpha S = 8\cos^2\theta_W \sin^2\theta_W \frac{m_Z^2}{\Lambda_{\text{IR}}^2}\frac{1}{Z} I,$$
$$\alpha T = \sin^2\theta_W \frac{m_Z^2}{\Lambda_{\text{IR}}^2}\frac{ky_1}{Z^2} I, \tag{27}$$

where y_1 is the position of the IR brane and the dimensionless integrals I and Z are defined as

$$I = k\int_0^{y_1} [(k(y_1 - y))^2] e^{2A(y)-2A(y_1)} dy,$$
$$Z = k\int_0^{y_1} dy \frac{h^2(y)}{h^2(y_1)} e^{-2A(y)+2A(y_1)}. \tag{28}$$

$h(y)$ is the profile of the vacuum expectation value and is given as

$$h(y) = h(y_1)e^{bk(y-y_1)}. \tag{29}$$

We find that the T parameter is enhanced by the volume factor in addition to being suppressed by two powers of Z. In RS models where $A(y) = ky$, $Z = 0.5$ for $b = 2$ and becomes smaller as the Higgs field approaches the IR brane ($b \to \infty$). This results in the enhancement of the T parameter, leading to stringent constraints on the KK scale. As a result, the authors of Refs. [36–38] considered an alternative solution by considering a modification of the line element in Eq. (15), where $A(y)$ is now given as

$$A(y) = ky - \frac{1}{\nu^2}\log\left(1 - \frac{y}{y_s}\right). \tag{30}$$

Note that $\nu \to \infty$ results in the RS limit. A consequence of this metric is that the singularity at the IR brane is shifted outside the patch between the IR and UV branes at $y_s = y_1 + \Delta$. Δ is the distance of the singularity from the IR brane. For the case where the hierarchy problem is solved, i.e., $A(y_1) \sim 36$, the position of the IR brane in the bulk y_1 is a function of ν, Δ. A smaller ν will in general result in a smaller volume factor y_1 and helps in ameliorating the constraints on the KK mass from the T parameter. Additionally, as noted in Refs. [36,37], this setup results in large values of Z for certain choices of the parameters ν, Δ, and b which help in reducing the KK scales so as to be within the reach of the LHC.

As before we perform an analysis to determine the parameter space of the $b - \Lambda_{\text{IR}}$ plane. We choose two sets of (ν, Δ) as follows:

(a) $\nu = 0.8$ and $\Delta = 1$. This corresponds to $y_1 = 30.60/k$ so that $A(y_1) \equiv 36$.
(b) $\nu = 1$ and $\Delta = 0.1$. This corresponds to $y_1 = 30.28/k$ so that $A(y_1) \equiv 36$.

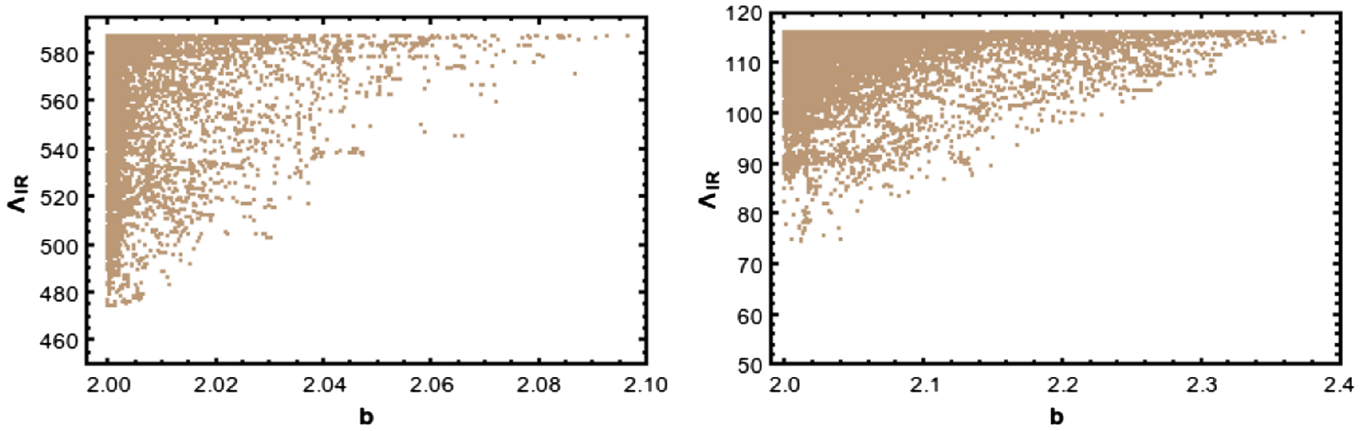

FIG. 4. Allowed parameter space in the $b - \Lambda_{\text{IR}}$ plane for the deformed metric. Λ_{IR} is in GeV. The left panel corresponds to $\nu = 0.8$ and $\Delta = 1$, while the right panel corresponds to $\nu = 1$ and $\Delta = 0.1$.

TABLE V. Fit values for the input and output observables for the deformed RS case. $b = 2.0006$ and $m^1_{kk} = 2.3$ TeV are obtained for the fit. $\nu = 0.8$ and $\Delta = \frac{1}{k}$ are chosen for the fit.

Input observables	m_Z	91.1813	G_F	1.1663785×10^{-5}
	$\alpha(m_Z)$	7.81663×10^{-3}	$m_t(m_t)$	173.12
	$\alpha_s(m_Z)$	0.119118	m_H	126.29
Output observables	m_W	80.419	Γ_Z	2.498
	σ_{had}	41.486	R_e	20.7381
	R_μ	20.7382	R_{tau}	20.785
	R_b	0.215	R_c	0.171
	$\sin^2\theta_e$	0.2314	$\sin^2\theta_b$	0.2328
	$\sin^2\theta_c$	0.2313	A^e_{FB}	0.0162
	A^b_{FB}	0.1032	A^c_{FB}	0.0737
	A_b	0.9346	A_c	0.6679
Model Parameters	b	2.00	m^1_{kk}	2.3 TeV

For the deformed metric, Λ_{IR} is related to the first m_{kk} scale by the following relation [36,37]:

$$m^1_{kk} \sim j_{0,1}\frac{A'(y_1)}{k}\Lambda_{\text{IR}}, \tag{31}$$

where $j_{0,1}$ is the first zero of the Bessel function $J_0(x)$. We scan the b parameter from 2 to 5 and Λ_{IR} is scanned from 50 to 587 GeV for case a), while it is scanned from 50 to 120 GeV for case b). The upper limit on Λ_{IR} corresponds to a KK mass of ~3 TeV. From the left panel of Fig. 4, a lowest value of $\Lambda_{\text{IR}} = 472.6$ GeV is obtained for $b = 2$ which corresponds to a first KK mass of about 2.3 TeV. For case b), depicted in the right panel of Fig. 4, a lowest value of $\Lambda_{\text{IR}} = 71.10$ GeV is obtained again for $b = 2$. This corresponds to a first KK mass of about 1.7 TeV for the gauge boson. Thus we see that for certain choices of the metric depending on the values (ν, Δ), the first KK mass of the gauge boson can be below 2 TeV. The fit values for the input and output observables are given in Table V. Case b) offers an advantage over case a) in terms of being a less fine-tuned model since the Λ_{IR} for the fit is small. The analysis can be repeated for different values of ν and Δ. For our analysis we fit the top-quark mass by $c_{Q_3} \sim 0.475$ and $c_t \sim -1$ with a choice of a $\mathcal{O}(1)$ Yukawa ~4.

The localization of the top doublet relatively near the UV brane is to minimize the correction to the Zbb vertex.

Fine-tuning: Due to the deformation in the metric, the Higgs mass in Eq. (26) can be generalized to [36,37,64]

$$m^2_H = \frac{2}{Z}(m_{\text{brane}} - m'_{\text{brane}})\frac{\Lambda^2_{\text{IR}}}{k} \quad \text{where}$$
$$Z = \int_0^{y_1}\frac{h^2(y)}{h^2(y_1)}e^{-2A(y)+2A(y_1)}. \tag{32}$$

For the normal RS case, $A(y) = ky$ and $Z = \frac{1}{2(a-1)}$, thus reducing to Eq. (26). In comparison to RS where $Z < 1$, certain choices of ν and δ result in $Z > 1$ which not only lowers the contribution to the T parameter in Eq. (27) but also helps in reducing the fine-tuning to obtain the Higgs mass. For instance, for the parameters in Table V, $Z = 2.6$, the tuning reduces to 0.018.

VI. CUSTODIAL RS

The custodial Randall Sundrum setup [31] contains an enlarged bulk gauged symmetry given by

$$\text{SU}(2)_L \times \text{SU}(2)_R \times \text{U}(1)_X \tag{33}$$

which restores the custodial symmetry in the RS setup for the Higgs potential. The corresponding gauge bosons are denoted by $W^{1,2,3}_{L\mu}$, $W^{1,2,3}_{R\mu}$, and X_μ, with $g_{5L,5R,5X}$ denoting the corresponding five-dimensional gauge couplings. In updating the electroweak constraints in this setup we follow the notation of Ref. [32].

The bulk symmetry is broken down to the Standard Model by considering the following boundary conditions for the gauge fields:

$$W^{1,2,3}_{L\mu}(++), \qquad B_\mu(++), \qquad W^{1,2}_{R\mu}(-+), \qquad Z'_\mu(-+), \tag{34}$$

with $+(-)$ denoting Neumann (Dirichlet) boundary conditions as before. The gauge fields B_μ and Z'_μ are defined as

$$B_\mu = \frac{g_{5X}W^3_{R\mu} + g_{5R}X_\mu}{\sqrt{g^2_{5R} + g^2_{5X}}}, \qquad Z'_\mu = \frac{g_{5R}W^3_{R\mu} - g_{5X}X_\mu}{\sqrt{g^2_{5R} + g^2_{5X}}}. \tag{35}$$

The $W^{1,2,3}_{L\mu}$ and B_μ possess zero modes corresponding to the SM $\text{SU}(2)_L$ and the $\text{U}(1)_Y$ gauge boson, respectively. The hypercharge coupling is given by $Y = 2(T^3_R + Q_X)$. After electroweak symmetry breaking, the electromagnetic charge is given by $Q_{\text{em}} = T^3_R + T^3_L + Q_X$. On the other hand, owing to the mixed boundary conditions of $W^{1,2}_{R\mu}$ and Z'_μ, they do not possess a zero mode.

The presence of new gauge bosons induces additional corrections to the T parameter but the S parameter remains unchanged. It is given as [11,15,37,66,67]

$$\alpha T = \frac{\sin^2\theta_W m_Z^2 y_1 k^2 e^{-2kR\pi}}{\Lambda_{\rm IR}^2}(\alpha_{hh} - \alpha'_{hh} - 2\alpha_{hf} + \alpha_{ff}), \tag{36}$$

where α'_{hh} is the bulk propagator for the bosons with $(-+)$ boundary conditions and is given as

$$\alpha'_{hh} = \int_0^{y_1} e^{2A(y)}(1-\Omega_h)^2. \tag{37}$$

The contributions to the T parameter due to the KK states of the SM as well as the new gauge bosons are very similar in magnitude. Recalling that the dominant contribution to the T parameter is due to α_{hh}, the presence of α'_{hh} nearly cancels this contribution, thus significantly lowering the constraint on the first KK scale of the gauge boson. As a result, the dominant constraint to the KK scale is due to the S parameter. To see the effects of a negligible T parameter on the fits we assume UV localized fermions to begin with. To obtain the plot for $b-\Lambda_{\rm IR}$ parameter space in the presence of custodial symmetry, we first evaluate the constraints at tree level. From the S-T plot in Fig. 1, the region around $T\sim 0$ would also necessitate the S parameter to be small, thereby pushing the KK scale up. Indeed, as is noted in the left panel of Fig. 5, a lowest value of $\Lambda_{\rm IR} = 1659$ GeV is obtained which translates into a lowest KK mass of around 4 TeV. While this case does better than the normal bulk RS scenario the first KK mass is still out of reach of the LHC.

The assumption of UV localized fermions is not sufficient to fit the top-quark mass as it would result in large $\mathcal{O}(1)$ Yukawa coupling. As a result the zero mode top doublet and the singlet must be moved closer to the IR brane ($c<0.5$) to increase overlap with the Higgs. This results in the shift of the coupling of b_L to the Z boson. The relative shift to b_L is given as [11,32]

$$\frac{\delta g_{b_L}}{g_{b_L}} = -v^2\frac{(g_L^2 T_L^3 - g_R^2 T_R^3)\alpha'_{hf} + (g_L^2 T_L^3 - (g')^2 Y)(\alpha_{hf} - \alpha_{hf}^{\rm UV} - \alpha'_{hf})}{1-\frac{2}{3}\sin^2\theta_W}. \tag{38}$$

The first term involving α'_{hf} will be significant in this case as the third-generation doublet is localized closer to the IR brane to fit the top-quark mass. In the second term however the presence of α'_{hf} and α_{hf} with a relative minus sign softens the impact of localization of the third generation on $\frac{\delta g_{b_L}}{g_{b_L}}$. The current constraints on the corrections to the Zb_Lb_L coupling pushes the limit obtained in the left panel of Fig. 5 to beyond 5 TeV. However it was observed in Ref. [68] that the dominant contribution due to the first term in Eq. (38) can be removed by assuming $T_L^3 = T_R^3$ and $g_L = g_R$, thus significantly softening the constraints on the KK mass from corrections to the $Zb\bar{b}$ vertex. This implies that the left-handed bottom must belong to bidoublets of $\mathrm{SU}(2)_L\times \mathrm{SU}(2)_R$. The bidoublets induce large negative contributions to the T parameter in most regions of the parameter space. The contribution is a function of $c_{Q_3,t}$ which are the localization parameters for the bidoublet and the singlet t_R. It was noted in Ref. [32] that the negative contribution decreases as the doublet and/or singlet are localized away from the IR brane. However, the top-quark mass as a function of $c_{Q_3,t}$ is given as

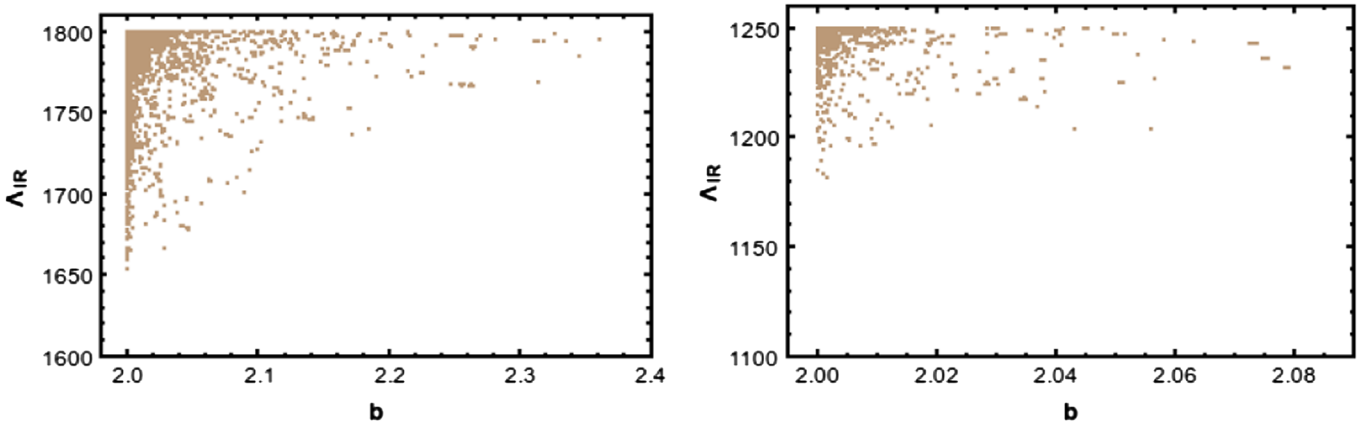

FIG. 5. The left panel shows the $b-\Lambda_{\rm IR}$ parameter space when just the tree-level computations of $S-T$ are taken into account. In the right panel, the loop contributions to the T parameter are also included. $\Lambda_{\rm IR}$ is in GeV.

TABLE VI. Fit values for the input and output observables. The corresponding RS parameters are $b = 2.0004$ and $m^1_{kk} = 2.9$ TeV. $\Lambda_{\rm IR}$ is in GeV. The loop contribution to the T parameter is ∼0.06.

Input observables	m_Z	91.1938	G_F	1.1663787×10^{-5}
	$\alpha(m_Z)$	7.81509×10^{-3}	$m_t(m_t)$	173.3499
	$\alpha_s(m_Z)$	0.119003	m_H	125.40
Output observables	m_W	80.347	Γ_Z	2.495
	$\sigma_{\rm had}$	41.471	R_e	20.736
	R_μ	20.736	$R_{\rm tau}$	20.783
	R_b	0.215	R_c	0.171
	$\sin^2\theta_e$	0.231	$\sin^2\theta_b$	0.233
	$\sin^2\theta_c$	0.2317	A^e_{FB}	0.0155
	A^b_{FB}	0.100	A^c_{FB}	0.072
	A_b	0.934	A_c	0.666
Model Parameters	b	2.00	m^1_{kk}	2.88 TeV

$$m_{\rm top} = \tilde{Y}^u_{3,3}\frac{v}{\sqrt{2}(\pi R)^{3/2}} \times \int_0^{\pi R} f_0^{(0)}(b,y) f_{1/2}^{(0)}(c_{Q_3},y) f_{1/2}^{(0)}(c_t,y), \quad (39)$$

where $Y^u_{3,3}$ is a dimensionless $\mathcal{O}(1)$ parameter. Choosing the bidoublet and the singlet to be localized away from the IR brane will result in the choice of a large $Y^u_{3,3} > 10$ to fit the top-quark mass and is not feasible. As a result the combination of $c_{Q_3,t}$ that induces a positive contribution to the T parameter is when $c_Q \leq 0$ and $c_t \sim [0.4, 0.5]$. As shown in Ref. [32], this choice of c parameters not only fits the top-quark mass but also gives a non-negative contribution to the T parameter.

A nonzero positive contribution to the T parameter would correspond to moving vertically up in the S-T plane in Fig. 1. The tilted orientation of the ellipse makes it possible to accommodate larger values of S, thereby helping to reduce the lower bound on the first KK mass. The right panel of Fig. 5 corresponds to the case where the loop-level contributions to the T parameter [32] have been turned on. In the figure we have assumed $\Delta T_{\rm loop} \leq 0.1$. We find that a minimum of $\Delta T_{\rm loop} \sim 0.06$ for $b = 2$ is required to lower the scale of the first KK gauge boson below 3 TeV. As b increases (corresponding to the Higgs moving further towards the IR brane) one can expect the minimum $\Delta T_{\rm loop}$ required to keep the KK scale below 3 TeV to increase. The fit values for the input and output observables are given in Table VI.

Fine-tuning: In this case too we find that the best fit to the precision data is when the brane mass parameter $b = 2$. The KK mass is lowered to 3 TeV, thus reducing the fine-tuning by an order of magnitude. As a result the cancellation between $m_{\rm brane}$ and $m'_{\rm brane}$ is of the order of 0.002

VII. CONCLUSIONS

There is a perception that in order for the Randall-Sundrum model to successfully address the gauge-hierarchy problem, the Higgs ought to be localized on the IR brane. It has been noted earlier [59,64] that this is not the case and our results bear this out. In fact, we find that even if we move the Higgs field off the IR brane, a solution to the gauge hierarchy problem is obtained as long as we have $b \geq 2$. Further, electroweak fits and the fine-tuning argument seem to prefer a b value very close to 2. In the dual CFT terminology, the Higgs field is a partially composite state [69,70]. This has to do with the exponential form of the scalar profiles which get pushed close to the IR brane for values of b greater than 2, so that from the point of view of the gauge hierarchy the Higgs is essentially IR localized. However, such a bulk Higgs differs from the brane-localized Higgs in the freedom that it offers in exploring the parameter space of the model when confronted with electroweak precision constraints.

A few remarks about the collider implications of bulk RS models are in order. Generically, in these models the gauge boson KK modes provide the most interesting signals, and of these the KK gluon is the most important [71–73]. The production cross section of the KK gauge boson modes is very small partly because of the couplings of these modes to the SM particles, but also because of the strong constraints on the masses of the KK modes coming from electroweak and flavor constraints. The cross sections for other KK modes (like those of the fermions) are even smaller than that of the gauge boson KK modes (except in some versions of the RS model where the Higgs is treated as a pseudo-Nambu-Goldstone boson). The collider tests of the bulk RS models are therefore difficult and several

TABLE VII. Summary of results for the various models at 3σ.

Model	m_{KK}(TeV)	b
Normal RS	5.9	2.00
Deformed RS ($\nu = 0.8$, $\Delta = 1$)	2.3	2.00
Deformed RS ($\nu = 1$, $\Delta = .1$)	1.7	2.00
Custodial RS	2.88	2.00

studies which propose probing alternative production channels have been presented [74,75], but the range of masses probed by these processes is just marginally larger than that allowed by precision constraints. In view of this, our results of the global fit for the deformed metric case are very encouraging. Unlike the custodial-symmetry case for which the global fits yield a bound on the mass of the first KK mode of about 2.9 TeV, one gets a lower bound of around 2.3 TeV at 3σ for the case of the deformed metric for $\nu = 0.8$ and $\Delta = 1$. This bound reduces to about 1.7 TeV when $\nu = 1$ and $\Delta = 0.1$. Table VII gives a summary of the results obtained. A collider analysis for such a class of models was done in Ref. [76]. The deformed metric model then is testable at the LHC at a statistically significant level and a more detailed study of the collider implications of this model is called for.

ACKNOWLEDGMENTS

A. I. and K. S. would like to thank the Centre for High Energy Physics, IISc for its hospitality during their visit where part of the discussions were conducted.

[1] L. Randall and R. Sundrum, A large mass hierarchy from a small extra dimension, Phys. Rev. Lett. **83**, 3370 (1999).
[2] T. Gherghetta and A. Pomarol, Bulk fields and supersymmetry in a slice of AdS, Nucl. Phys. **B586**, 141 (2000).
[3] T. Gherghetta, TASI lectures on a holographic view of beyond the Standard Model physics, arXiv:1008.2570.
[4] K. Agashe, A. Delgado, and R. Sundrum, Grand unification in RS1, Ann. Phys. (Amsterdam) **304**, 145 (2003).
[5] M. E. Peskin and T. Takeuchi, Estimation of oblique electroweak corrections, Phys. Rev. D **46**, 381 (1992).
[6] H. Davoudiasl, J. Hewett, and T. Rizzo, Bulk gauge fields in the Randall-Sundrum model, Phys. Lett. B **473**, 43 (2000).
[7] S. Chang, J. Hisano, H. Nakano, N. Okada, and M. Yamaguchi, Bulk standard model in the Randall-Sundrum background, Phys. Rev. D **62**, 084025 (2000).
[8] S. J. Huber and Q. Shafi, Higgs mechanism and bulk gauge boson masses in the Randall-Sundrum model, Phys. Rev. D **63**, 045010 (2001).
[9] C. Csaki, J. Erlich, and J. Terning, The effective Lagrangian in the Randall-Sundrum model and electroweak physics, Phys. Rev. D **66**, 064021 (2002).
[10] G. Burdman, Constraints on the bulk standard model in the Randall-Sundrum scenario, Phys. Rev. D **66**, 076003 (2002).
[11] A. Delgado and A. Falkowski, Electroweak observables in a general 5D background, J. High Energy Phys. 05 (2007) 097.
[12] K. Agashe, G. Perez, and A. Soni, Flavor structure of warped extra dimension models, Phys. Rev. D **71**, 016002 (2005).
[13] S. J. Huber and Q. Shafi, Fermion masses, mixings and proton decay in a Randall-Sundrum model, Phys. Lett. B **498**, 256 (2001).
[14] C. Delaunay, O. Gedalia, S. J. Lee, G. Perez, and E. Ponton, Ultra visible warped model from flavor triviality and improved naturalness, Phys. Rev. D **83**, 115003 (2011).
[15] S. Casagrande, F. Goertz, U. Haisch, M. Neubert, and T. Pfoh, Flavor physics in the Randall-Sundrum model: I. Theoretical setup and electroweak precision tests, J. High Energy Phys. 10 (2008) 094.
[16] M. Bauer, S. Casagrande, U. Haisch, and M. Neubert, Flavor physics in the Randall-Sundrum model: II. Tree-level weak-interaction processes, J. High Energy Phys. 09 (2010) 017.
[17] Y. Grossman and M. Neubert, Neutrino masses and mixings in nonfactorizable geometry, Phys. Lett. B **474**, 361 (2000).
[18] R. Kitano, Lepton flavor violation in the Randall-Sundrum model with bulk neutrinos, Phys. Lett. B **481**, 39 (2000).
[19] S. J. Huber and Q. Shafi, Neutrino oscillations and rare processes in models with a small extra dimension, Phys. Lett. B **512**, 365 (2001).
[20] S. J. Huber and Q. Shafi, Majorana neutrinos in a warped 5-D standard model, Phys. Lett. B **544**, 295 (2002).
[21] S. J. Huber and Q. Shafi, Seesaw mechanism in warped geometry, Phys. Lett. B **583**, 293 (2004).
[22] K. Agashe, A. E. Blechman, and F. Petriello, Probing the Randall-Sundrum geometric origin of flavor with lepton flavor violation, Phys. Rev. D **74**, 053011 (2006).
[23] A. L. Fitzpatrick, L. Randall, and G. Perez, Flavor anarchy in a Randall-Sundrum model with 5D minimal flavor violation and a low Kaluza-Klein scale, Phys. Rev. Lett. **100**, 171604 (2008).
[24] M.-C. Chen and H.-B. Yu, Minimal flavor violation in the lepton sector of the Randall-Sundrum model, Phys. Lett. B **672**, 253 (2009).
[25] K. Agashe, T. Okui, and R. Sundrum, A common origin for neutrino anarchy and charged hierarchies, Phys. Rev. Lett. **102**, 101801 (2009).
[26] P. R. Archer, The fermion mass hierarchy in models with warped extra dimensions and a bulk Higgs, J. High Energy Phys. 09 (2012) 095.
[27] A. M. Iyer and S. K. Vempati, Lepton masses and flavor violation in Randall-Sundrum model, Phys. Rev. D **86**, 056005 (2012).
[28] A. M. Iyer and S. K. Vempati, Bulk Majorana mass terms and Dirac neutrinos in the Randall-Sundrum model, Phys. Rev. D **88**, 073005 (2013).
[29] A. M. Iyer, Revisiting neutrino masses from Planck scale operators, Phys. Rev. D **89**, 116008 (2014).
[30] T. Gherghetta, A holographic view of beyond the Standard Model physics, in *Physics of the Large and the Small, TASI 09, Proceedings of the Theoretical Advanced Study Institute in Elementary Particle Physics, Boulder, Colorado, USA,*

1–26 June, 2009 (World Scientific, Singapore, 2011), p. 165.
[31] K. Agashe, A. Delgado, M. J. May, and R. Sundrum, RS1, custodial isospin and precision tests, J. High Energy Phys. 08 (2003) 050.
[32] M. S. Carena, E. Ponton, J. Santiago, and C. E. Wagner, Light Kaluza-Klein states in Randall-Sundrum models with custodial SU(2), Nucl. Phys. **B759**, 202 (2006).
[33] M. S. Carena, E. Ponton, J. Santiago, and C. Wagner, Electroweak constraints on warped models with custodial symmetry, Phys. Rev. D **76**, 035006 (2007).
[34] P. R. Archer, M. Carena, A. Carmona, and M. Neubert, Higgs production and decay in models of a warped extra dimension with a bulk Higgs, J. High Energy Phys. 01 (2015) 060.
[35] A. Falkowski and M. Perez-Victoria, Electroweak breaking on a soft wall, J. High Energy Phys. 12 (2008) 107.
[36] J. A. Cabrer, G. von Gersdorff, and M. Quiros, Warped electroweak breaking without custodial symmetry, Phys. Lett. B **697**, 208 (2011).
[37] J. A. Cabrer, G. von Gersdorff, and M. Quiros, Suppressing electroweak precision observables in 5D warped models, J. High Energy Phys. 05 (2011) 083.
[38] J. A. Cabrer, G. von Gersdorff, and M. Quiros, Warped 5D Standard Model consistent with EWPT, Fortschr. Phys. **59**, 1135 (2011).
[39] A. Carmona, E. Ponton, and J. Santiago, Phenomenology of non-custodial warped models, J. High Energy Phys. 10 (2011) 137.
[40] M. S. Carena, A. Delgado, E. Ponton, T. M. Tait, and C. Wagner, Precision electroweak data and unification of couplings in warped extra dimensions, Phys. Rev. D **68**, 035010 (2003).
[41] K. Agashe, M. Bauer, F. Goertz, S. J. Lee, L. Vecchi, L.-T. Wang, and F. Yu, Constraining RS models by future flavor and collider measurements: A Snowmass whitepaper, Report No. FERMILAB-CONF-13-435-T, arXiv:1310.1070.
[42] S. Fichet and G. von Gersdorff, Anomalous gauge couplings from composite Higgs and warped extra dimensions, J. High Energy Phys. 03 (2014) 102.
[43] B. M. Dillon and S. J. Huber, Non-custodial warped extra dimensions at the LHC?, J. High Energy Phys. 06 (2015) 066.
[44] J. D. Wells and Z. Zhang, Precision electroweak analysis after the Higgs boson discovery, Phys. Rev. D **90**, 033006 (2014).
[45] A. Falkowski and F. Riva, Model-independent precision constraints on dimension-6 operators, J. High Energy Phys. 02 (2015) 039.
[46] F. James and M. Roos, MINUIT: A system for function minimization and analysis of the parameter errors and correlations, Comput. Phys. Commun. **10**, 343 (1975).
[47] S. Schael *et al.*, Precision electroweak measurements on the Z resonance, Phys. Rep. **427**, 257 (2006).
[48] J. Beringer *et al.*, Review of particle physics, Phys. Rev. D **86**, 010001 (2012).
[49] ATLAS, CDF, CMS, and D0 Collaborations, First combination of Tevatron and LHC measurements of the top-quark mass, Report Nos. ATLAS-CONF-2014-008, CDF-NOTE-11071, CMS-PAS-TOP-13-014, D0-NOTE-6416, FERMILAB-TM-2582-E 2014, arXiv:1403.4427.
[50] Tevatron Electroweak Working Group, 2012 update of the combination of CDF and D0 results for the mass of the W boson, Report No. FERMILAB-TM-2532-E 2012, arXiv:1204.0042.
[51] R. Alonso, E. E. Jenkins, A. V. Manohar, and M. Trott, Renormalization group evolution of the Standard Model dimension six operators III: Gauge coupling dependence and phenomenology, J. High Energy Phys. 04 (2014) 159.
[52] J. Elias-Mir, C. Grojean, R. S. Gupta, and D. Marzocca, Scaling and tuning of EW and Higgs observables, J. High Energy Phys. 05 (2014) 019.
[53] B. Henning, X. Lu, and H. Murayama, How to use the Standard Model effective field theory, arXiv:1412.1837.
[54] L. Berthier and M. Trott, Towards consistent electroweak precision data constraints in the SMEFT, J. High Energy Phys. 05 (2015) 024.
[55] M. E. Peskin and T. Takeuchi, A new constraint on a strongly interacting Higgs sector, Phys. Rev. Lett. **65**, 964 (1990).
[56] J. Ellis, V. Sanz, and T. You, The effective Standard Model after LHC Run I, J. High Energy Phys. 03 (2015) 157.
[57] M. Baak, M. Goebel, J. Haller, A. Hoecker, D. Kennedy, R. Kogler, K. Moenig, M. Schott, and J. Stelzer, The electroweak fit of the Standard Model after the discovery of a new boson at the LHC, Eur. Phys. J. C **72**, 2205 (2012).
[58] J. Hewett, F. Petriello, and T. Rizzo, Precision measurements and fermion geography in the Randall-Sundrum model revisited, J. High Energy Phys. 09 (2002) 030.
[59] M. A. Luty and T. Okui, Conformal technicolor, J. High Energy Phys. 09 (2006) 070.
[60] H. Davoudiasl, B. Lillie, and T. G. Rizzo, Off-the-wall Higgs in the universal Randall-Sundrum model, J. High Energy Phys. 08 (2006) 042.
[61] J. A. Cabrer, G. von Gersdorff, and M. Quiros, Warped electroweak breaking without custodial symmetry, Phys. Lett. B **697**, 208 (2011).
[62] G. Perez and L. Randall, Natural neutrino masses and mixings from warped geometry, J. High Energy Phys. 01 (2009) 077.
[63] A. M. Iyer and S. K. Vempati, Lepton masses and flavor violation in Randall-Sundrum model, Phys. Rev. D **86**, 056005 (2012).
[64] M. Quiros, Higgs bosons in extra dimensions, Mod. Phys. Lett. A **30**, 1540012 (2015).
[65] A. L. Fitzpatrick, J. Kaplan, E. Katz, and L. Randall, Decoupling of high dimension operators from the low energy sector in holographic models, arXiv:1304.3458.
[66] H. Davoudiasl, S. Gopalakrishna, E. Ponton, and J. Santiago, Warped 5-dimensional models: Phenomenological status and experimental prospects, New J. Phys. **12**, 075011 (2010).
[67] S. Casagrande, F. Goertz, U. Haisch, M. Neubert, and T. Pfoh, The custodial Randall-Sundrum model: From precision tests to Higgs physics, J. High Energy Phys. 09 (2010) 014.
[68] K. Agashe, R. Contino, L. Da Rold, and A. Pomarol, A custodial symmetry for $Zb\bar{b}$, Phys. Lett. B **641**, 62 (2006).

[69] B. Batell and T. Gherghetta, Holographic mixing quantified, Phys. Rev. D **76**, 045017 (2007).
[70] B. Batell and T. Gherghetta, Warped phenomenology in the holographic basis, Phys. Rev. D **77**, 045002 (2008).
[71] K. Agashe, A. Belyaev, T. Krupovnickas, G. Perez, and J. Virzi, LHC signals from warped extra dimensions, Phys. Rev. D **77**, 015003 (2008).
[72] K. Agashe, H. Davoudiasl, S. Gopalakrishna, T. Han, G.-Y. Huang, G. Perez, Z.-G. Si, and A. Soni, LHC signals for warped electroweak neutral gauge bosons, Phys. Rev. D **76**, 115015 (2007).
[73] K. Agashe, S. Gopalakrishna, T. Han, G.-Y. Huang, and A. Soni, LHC signals for warped electroweak charged gauge bosons, Phys. Rev. D **80**, 075007 (2009).
[74] M. Guchait, F. Mahmoudi, and K. Sridhar, Associated production of a Kaluza-Klein excitation of a gluon with a $t\bar{t}$ pair at the LHC, Phys. Lett. B **666**, 347 (2008).
[75] B. C. Allanach, F. Mahmoudi, J. P. Skittrall, and K. Sridhar, Gluon-initiated production of a Kaluza-Klein gluon in a Bulk Randall-Sundrum model, J. High Energy Phys. 03 (2010) 014.
[76] J. de Blas, A. Delgado, B. Ostdiek, and A. de la Puente, LHC signals of non-custodial warped 5D models, Phys. Rev. D **86**, 015028 (2012).